

Developing a Battery Discharge Regulator Using Fuzzy Logic to Guarantee the Lowest Output Current Ripple for an Electrical Power System in a Geostationary Satellite

Sannidhi Mohan kumar¹, U. Lakshmi²

¹M.Tech(PSA), EEE, Sanketika vidya parishad engineering college., India

²Assistant professor nedi pg scholar, EEE, Sanketika vidya parishad engineering college, India

E-mail: ¹smohankumar917@gmail.com , ²ulakshmi27795@gmail.com

ABSTRACT:

The conventional Weinberg converter is primarily used in battery discharge regulators (BDR), which are parts of the overall electrical power system for geostationary satellites. This is because of its high efficiency, continuous input and output current, and soft switching of its switches and diodes. Still, one major issue with this converter is that when its output diodes are commutating, there is a significant amount of output current ripple. As a result, there is a significant ripple in the output voltage and root mean square (RMS) current. This might have a direct impact on the bus capacitors' lifespan and total capacitance, which would then have an impact on the geostationary satellite's size and longevity. Therefore, while building the electrical power system for a geostationary satellite, decreasing the ripple in the BDR's output current is crucial.

Consequently, in order to lower the output voltage ripple and output current ripple, this research suggests an enhanced Weinberg converter. In particular, the suggested converter decreases the magnetizing current offset of the coupled inductor in addition to having a lower output current and voltage ripple than the standard converter. Additionally, it can achieve high efficiency and soft switch all switches, just like a normal converter, without having to deal with the diodes' reverse recovery issue. Overall, test findings from a prototype with a 750 W rating validate the suggested converter.

1. INTRODUCTION:

The market for satellite data services has expanded dramatically in recent years. Consequently, private enterprises are now in charge of satellite development initiatives, which were previously overseen by government organizations [1], [2].

As a result, the need for satellites with different missions

is gradually growing. Generally speaking, geostationary satellites are employed for a number of purposes, including communication, navigation, and weather observation. More specifically, a higher-quality and more capacious power system is needed as satellite missions become more varied and sophisticated, which could result in an increase in the satellite's weight [3, [4], [5], [6], [7], [8], [9], [10]. Thus, in order to lower launch costs and meet the growing need for power, geostationary satellites must have a lightweight, high-power density power system [11]. Remarkably, a number of research have e been carried out to accomplish the high-power density, miniaturization, and light weight of geostationary satellites [12], [13], [14], [15], [16], [17], and [18]. Among the subsystems that comprise the geostationary satellite, the electrical power system must weigh less in order to facilitate the shrinking and light weighting of the spacecraft.

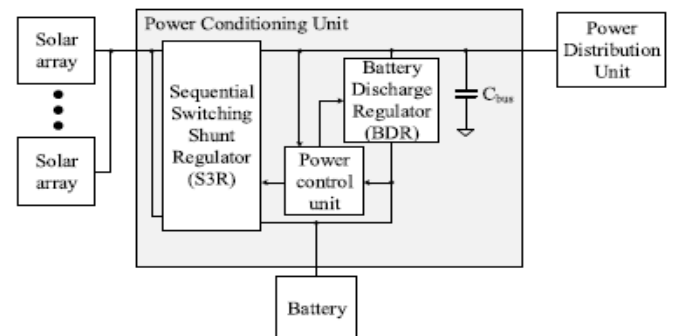


FIGURE 1. The sequential switching shunt regulator (S3R) & battery discharge regulator (BDR) topology for regulated bus voltage in the geostationary satellite.

In general, a controlled bus that keeps the bus voltage constant for a reliable power supply is the essential component of the electrical power system of geostationary satellites [19], [20]. More specifically, the electrical power system's power-conditioning unit (PCU) precisely and steadily regulates the bus voltage. The battery discharge regulator (BDR) topology and sequential switching shunt regulator (S3R) for the

regulated bus voltage in geostationary satellites are depicted in Fig. 1 [21]. The PCU is made up of an S3R, a BDR, a power control unit, and a bus capacitor, as seen in Fig. 1 [22, 23]. The PCU provides the electrical power required for the bus, charges the battery, and receives the power produced by the solar array during the sun time. But, because the solar array cannot produce any electricity during the eclipse, the BDR uses the battery's stored energy to power the bus. Furthermore, multiple-bus capacitors are needed to keep the bus voltage at a steady power level with a slight ripple.

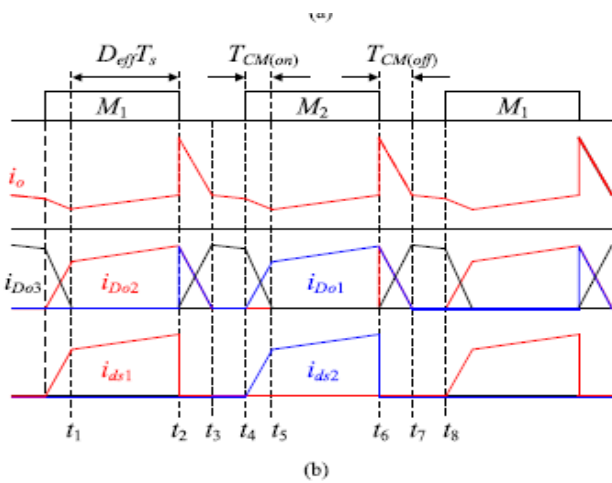
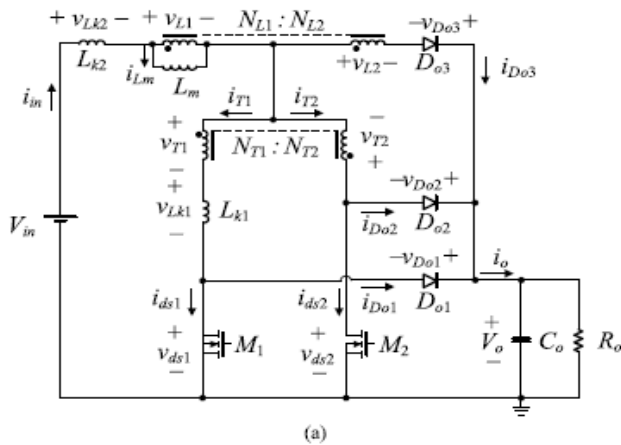


FIGURE 2. The circuit diagram and key operation waveforms of the conventional Weinberg converter

- (a) Conventional Weinberg converter circuit diagram,
- (b) The key waveforms of the current.

As a result, the huge volume of bus capacitors in the PCU may be reduced in order to miniaturize the electrical power system. Additionally, the PCU's bus capacitor is linked to the BDR's output, and the bus voltage is higher than the battery voltage, which serves as the BDR's input. Thus, the BDR is implemented via a step-up converter. Due to the numerous benefits, it offers—a list

of which is provided below—the typical Weinberg converter, one of the different step-up converters is primarily utilized in BDRs for geostationary satellites. It is depicted in Fig. 2(a)W [25], [26], [27], [24], [25].

The constant input and output currents lessen the strain on the battery and bus capacitor.

The leakage inductance enables the semiconductor device to operate in soft switching mode, resulting in excellent efficiency. The size of the magnetic components can be reduced because the working frequency is double that of the switching frequency.

Because all switches' voltages can be clamped to the output voltage, the voltage strains on the switches are low, negating the need for a snubber.

The traditional Weinberg converter offers a number of benefits, as previously mentioned. It does, however, have certain disadvantages, as Fig. 2(b) illustrates. Specifically, when all switches are off, the output current rises quickly, leading to a considerable increase in output current ripple. Furthermore, this results in a significant increase in both the output voltage ripple and the root mean square (RMS) current passing through the output capacitor. Furthermore, when the load current rises, these issues get worse. As a result, in order to tackle these issues, a high number of output capacitors are needed, which could increase the geostationary satellite's weight and volume.

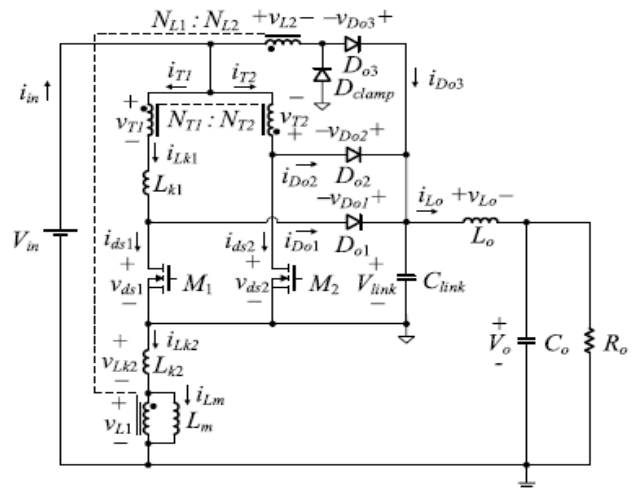


FIGURE 3. The circuit diagram of the proposed converter.

Therefore, an enhanced Weinberg converter is suggested, as seen in Fig. 3, to overcome the aforementioned problems. Specifically, the suggested converter uses a small link capacitor Clink and a small

output inductor L_o , but otherwise shares a topological structure with the standard converter. With the aid of the inductor L_o , it thus does not experience significant output current ripple problems while all switches are off. Furthermore, it can maintain a consistent amount of output current and voltage ripple independent of the load current, which can drastically lower the quantity of output capacitors needed compared to a typical converter.

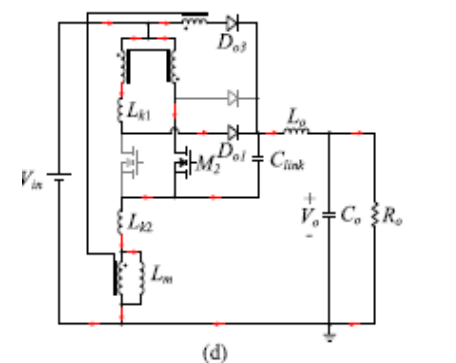
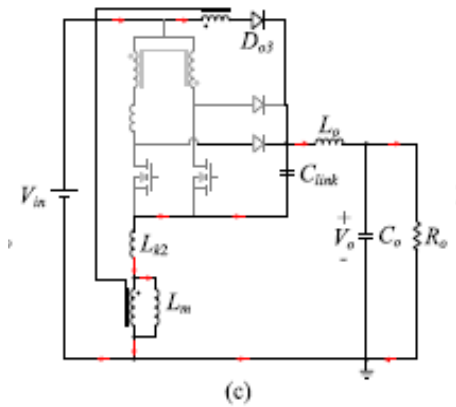
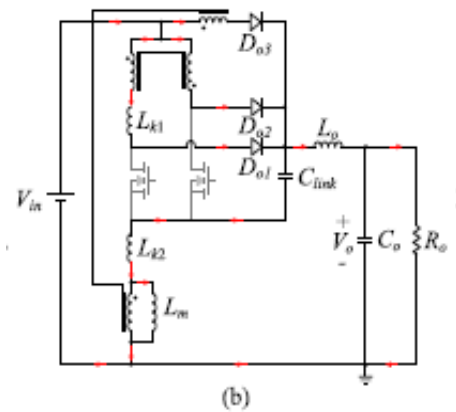
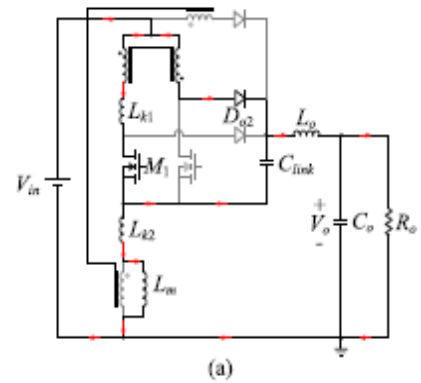
Because the magnetizing inductor current of the coupled inductor drops by the same amount as the load current, the suggested converter can also lower the size of the coupled inductor's magnetic core. Furthermore, by ensuring soft switching, the leakage inductors of the suggested converter can lessen the turn-on loss of every switch in addition to preventing reverse recovery issues with every diode. For this reason, the suggested converter has the advantages of low noise and high efficiency.

In the meantime, the output voltage is clamped to the diode D_{o3} 's voltage ringing by inserting the DC lamp, as seen in Fig. 3. However, as it has little bearing on how the converter operates, it is disregarded in the mode analysis and detailed analysis.

2. OPERATIONAL PRINCIPLES:

The suggested converter uses two switches with the same duty cycle (D), M_1 and M_2 , to function in an alternative fashion. Additionally, the following presumptions are made in order to facilitate an investigation of the operation of the suggested converter.

- The transformer's magnetizing inductor is big enough to be disregarded, and its turn ratio is $N_1:N_2 = 1:1$.
- The coupled inductor has a turn ratio of $N_{L1}:N_{L2} = 1:1$, and the magnetizing inductor is represented by L_m .
- The lumped leakage inductor, or transformer leakage inductor, is represented by L_{k1} , which is reflected on the left side of the transformer.
- L_{k2} , the lumped leakage inductor reflected on the N_{L1} side, is the leakage inductor of the coupled inductor.
- The three output diodes (D_{o1} , D_{o2} , and D_{o3}) and the two switches (M_1 and M_2) are perfect.
- As the average voltage across the inductors is zero, the voltage V_{ink} is equal to V_o at steady-state.
- The link capacitor C_{link} and output capacitor C_o are large enough to be considered as voltage sources V_{ink} and V_o , respectively.



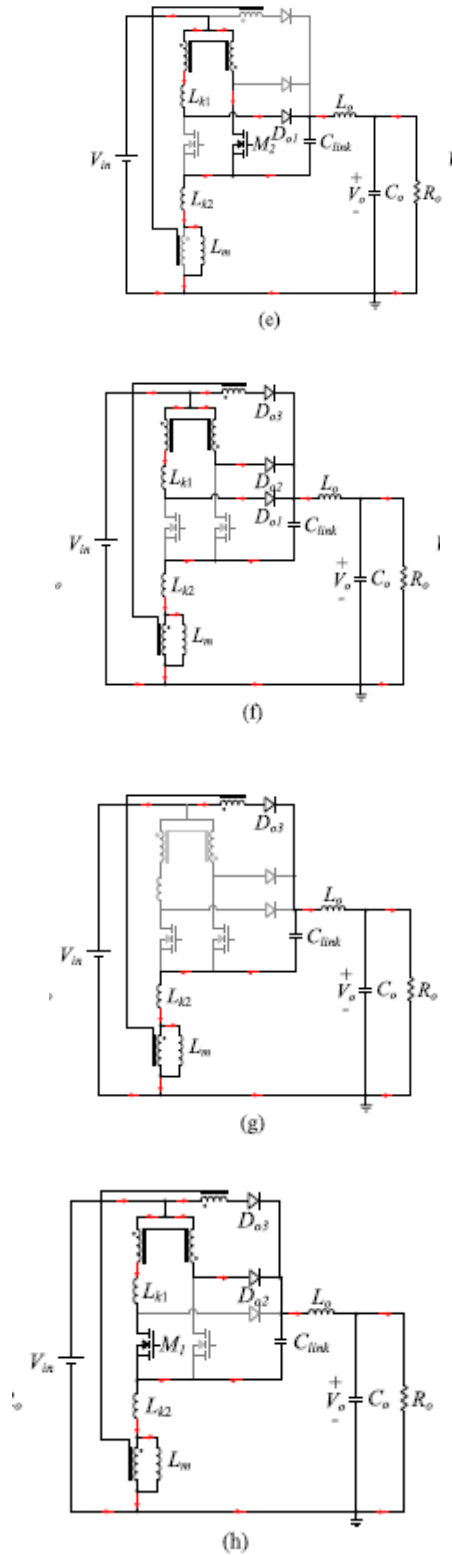


FIGURE 4. The circuit operation of the proposed converter during one period (a) Mode 1 (t1-t2), (b) Mode 2 (t2-t3), (c) Mode 3 (t3-t4), (d) Mode 4 (t4-t5), (e) Mode 5 (t5-t6), (f) Mode 6 (t6-t7), (g) Mode 7 (t7-t8), (h) Mode 8 (t8-t9).

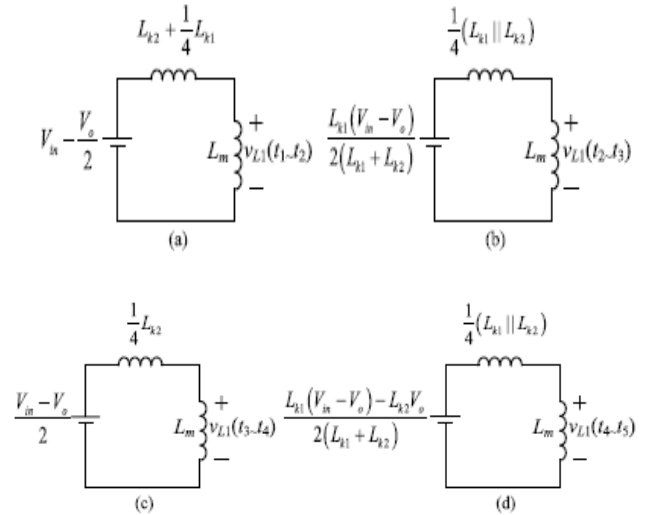


FIGURE 5. The equivalent circuits for each operation mode of the proposed converter (a) Mode 1 (t1-t2), (b) Mode 2 (t2-t3), (c) Mode 3 (t3-t4), (d) Mode 4 (t4-t5).

The suggested converter functions in eight modes, as depicted in Fig. 4, depending on the condition of the switches and diodes.

Fig. 5 depicts the equivalent circuits from mode 1 to mode 4 of the proposed converter, assuming that L_o is sufficiently greater than $L_{k1}/4$ and $L_{k2}/2$. Furthermore, the operation key waveforms of the suggested converter are displayed in Fig. 6. Furthermore, Fig. 3 displays the voltage that is supplied to each component as well as the current that passes through it.

Mode 1 [t1-t2]: This mode begins when the commutation between D_{o2} and D_{o3} ends at t_1 , and D_{o3} is turned off. In this mode, v_{L1} ($= v_{L2}$) applied to the coupled inductor can be derived as follows from Fig. 5(a).

$$v_{L1}(t) = \frac{L_m(4V_{in}-2V_o)}{4L_m+4L_{k2}+L_{k1}} \quad (1)$$

$$v_{Lk1}(t) = \frac{L_{k1}(2V_{in}-V_o)}{4L_m+4L_{k2}+L_{k1}} \quad (2)$$

$$v_{Lk2}(t) = \frac{L_{k2}(4V_{in}-V_o)}{4L_m+4L_{k2}+L_{k1}} \quad (3)$$

$$v_{L_o}(t) = \frac{(L_m+L_{k2})(4V_{in}-2V_o)}{4L_m+4L_{k2}+L_{k1}} \quad (4)$$

$$v_{D_{o3}}(t) = \frac{2L_mV_{in}+L_{k2}V_o}{4(L_m+L_{k2})} \quad (5)$$

Using (1) – (4), the currents flowing through L_m , L_{k1} , and L_o can be determined as follows:

$$i_{Lm}(t) = \frac{4V_{in}-2V_o}{4L_m+4L_{k2}+L_{k1}}(t - t1) + i_{Lm}(t1) \quad (6)$$

$$i_{Lk}(t) = \frac{2V_{in}-V_o}{4L_m+4L_{k2}+L_{k1}}(t - t1) + i_{Lk1}(t1) \quad (7)$$

$$i_{Lo}(t) = \frac{(L_m+L_{k2})(4V_{in}-2V_o)}{L_o(4L_m+4L_{k2}+L_{k1})}(t - t1) + i_{Lo}(t1) \quad (8)$$

In this mode, since Do3 is blocked, i_{Lk2} is equal to i_{Lm} .

Mode 2 [t2-t3]:

v_{ds1} rises from zero to $V_{link} = V_o$ when M1 is turned off at t_2 . Do1 is turned on and commutation between Do1, Do2, and Do3 occurs when v_{ds1} approaches $V_{link} = V_o$ begins. Furthermore, the following can be used to get $v_{L1} (= v_{L2})$ from Fig. 5(b).

$$v_{L1}(t) = \frac{2L_m L_{k1}(V_{in}-V_o)}{4L_m(L_{k1}+L_{k2})+L_{k1}L_{k2}} \quad (9)$$

If $4L_m$ in (9) is big enough compared to $L_{k1}||L_{k2}$, then v_{L1} can be expressed as $L_{k1}(V_{in}-V_o)/(2L_{k1}+2L_{k2})$. Furthermore, according to KVL, $v_{Lo} = V_{in}-V_o-v_{L2}$; $v_{T1} (= v_{T2}) = -v_{L2}$; $v_{Lk1} = 2v_{L2}$; and $v_{Lk2} = V_{in}-V_o-v_{L1}-v_{L2}$ since Do1 and Do2 are conducting. As a result, the following is how v_{Lk1} , v_{Lk2} , and v_{Lo} are derived:

$$v_{Lk1}(t) = \frac{L_{k1}(V_{in}-V_o)}{(L_{k1}+L_{k2})} \quad (10)$$

$$v_{Lk2}(t) = \frac{L_{k2}(V_{in}-V_o)}{(L_{k1}+L_{k2})} \quad (11)$$

$$v_{Lo}(t) = \frac{(L_{k1}+L_{k2})(V_{in}-V_o)}{2(L_{k1}+L_{k2})} \quad (12)$$

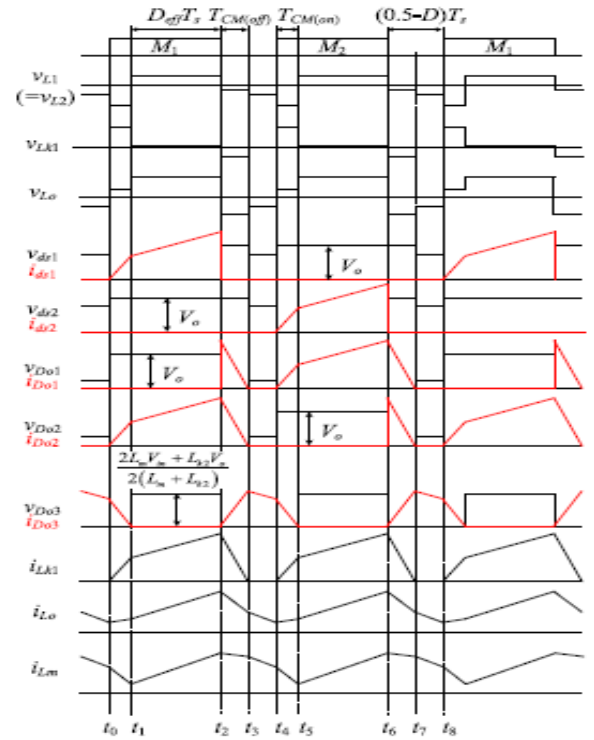


FIGURE 6. The key operation waveforms of the proposed converter.

It is possible to express the currents passing through L_m , L_{k1} , L_{k2} , and L_o using the voltages (9) through (12) that were previously determined as follows:

$$i_{Lm}(t) = \frac{L_{k1}(V_{in}-V_o)}{2L_m(L_{k1}+L_{k2})}(t - t2) + i_{Lm}(t2) \quad (13)$$

$$i_{Lk1}(t) = \frac{(V_{in}-V_o)}{(L_{k1}+L_{k2})}(t - t2) + i_{Lk1}(t2) \quad (14)$$

$$i_{Lk2}(t) = \frac{(V_{in}-V_o)}{(L_{k1}+L_{k2})}(t - t2) + i_{Lk2}(t2) \quad (15)$$

$$i_{Lo}(t) = \frac{(L_{k1}+2L_{k2})(V_{in}-V_o)}{2L_o(L_{k1}+L_{k2})}(t - t2) + i_{Lo}(t2) \quad (16)$$

Additionally, since in the prior mode $i_{Lm} = i_{Lk2}$, $i_{Lm}(t2) = i_{Lk2}(t2)$. Additionally, Kirchhoff's current law states that $i_{Do3} = i_{Lm}-i_{Lk2}$. (KCL). Consequently, i_{Do3} steadily rises. Based on (9) and (12). In the meantime, according to (11) $i_{Lk1} (= i_{Do1} = i_{Do2})$ steadily declines. The commutation between Do1, Do2, and Do3 so begins. The diode commutation procedure stops and Do1 and Do2 are stopped when i_{Do1} and i_{Do2} reach zero. Furthermore, there is no issue with Do1 and Do2's reverse recovery because they are softly switched off.

Unlike the typical converter, the suggested converter does not appreciably enhance the output current ripple because of the output inductor L_o , especially in this mode.

Mode 3 [t3–t4]: In this mode, i_{Lk1} is zero and the input current passes through $Do3$, as $Do1$ and $Do2$ are blocked. Furthermore, the energy that has been stored in L_m is moved to the output. v_{L1} ($= v_{L2}$) can be obtained as follows from Fig. 5(c).

$$V_{L1}(t) = \frac{2L_m(V_{in}-V_o)}{4L_m+L_{k2}} \quad (17)$$

By KVL, $v_{Lo} = V_{in}-V_o-v_{L2}$ and $v_{Lk2} = V_{in}-V_o-v_{L1}-v_{L2}$. Therefore, according to (17), v_{Lk2} and v_{Lo} can be expressed as follows V .

$$V_{Lk2}(t) = \frac{L_{k2}(V_{in}-V_o)}{4L_m+L_{k2}} \quad (18)$$

$$V_{Lo}(t) = \frac{(L_m+L_{k2})(4V_{in}-2V_o)}{4L_m+L_{k2}+L_{k1}} \quad (19)$$

Here is an expression for the current passing through L_m , L_{k2} , and L_o based on the previously derived (17)–(19):

$$i_{Lm}(t) = \frac{2(V_{in}-V_o)}{4L_m+L_{k2}}(t-t_3) + i_{Lm}(t_3) \quad (20)$$

$$i_{Lk2}(t) = \frac{(V_{in}-V_o)}{4L_m+L_{k2}}(t-t_3) + i_{Lk2}(t_3) \quad (21)$$

$$i_{Lo}(t) = \frac{(2L_m+L_{k2})(V_{in}-V_o)}{L_o(4L_m+L_{k2})}(t-t_3) + i_{Lo}(t_3) \quad (22)$$

Similar to the preceding mode, mode 3 terminates upon turning on $M2$. $i_{Do3} = i_{Lm}-i_{Lk2}$.

Mode 4 [t4–t5]: The transformer conducts current when $M2$ is activated at $t4$. As a result, v_{ds1} and v_{Do2} are clamped to $V_{link} = V_o$ and $Do1$ conducts. v_{L1} ($= v_{L2}$) can be obtained as follows from Fig. 5(d)

$$V_{L1}(t) = \frac{L_{k1}(V_{in}-V_o)-L_{k2}V_o}{2(L_{k1}+L_{k2})} \quad (23)$$

KVL states that v_{T1} ($= v_{T2}$) $= -V_o-v_{L1}$, $v_{Lk1} = -V_o-v_{T1}-v_{T2}$, and $v_{Lk2} = V_{in}+v_{T2}-v_{L1}$. $v_{Lo} = V_{in}-V_o-v_{L1}$. Consequently, the following voltages are across L_{k1} , L_{k2} , and L_o .

$$V_{Lk1}(t) = \frac{L_{k1}V_{in}}{(L_{k1}+L_{k2})} \quad (24)$$

$$V_{Lk2}(t) = \frac{L_{k2}V_{in}}{(L_{k1}+L_{k2})} \quad (25)$$

$$V_{Lo}(t) = \frac{L_{k1}(V_{in}-V_o)+L_{k2}(2V_{in}-V_o)}{2(L_{k1}+L_{k2})} \quad (26)$$

($V_{in} = 36$ V, $V_o = 50$ V, $P_o = 750$ W).

The currents flowing through L_m , L_{k1} , L_{k2} , and L_o are as follows, deduced from previously

(23) – (26):

$$i_{Lm}(t) = \frac{L_{k1}(V_{in}-V_o)-L_{k2}V_o}{2L_m(L_{k1}+L_{k2})}(t-t_3) + i_{Lm}(t_3) \quad (27)$$

$$i_{Lk1}(t) = \frac{V_{in}}{(L_{k1}+L_{k2})}(t-t_4) + i_{Lk1}(t_4) \quad (28)$$

$$i_{Lk2}(t) = \frac{V_{in}}{(L_{k1}+L_{k2})}(t-t_4) + i_{Lk2}(t_4) \quad (29)$$

$$i_{Lo}(t) = \frac{L_{k1}(V_{in}-V_o)+L_{k2}(2V_{in}-V_o)}{2L_o(L_{k1}+L_{k2})}(t-t_4) + i_{Lo}(t_4) \quad (30)$$

According to KCL, i_{Do1} in this mode equals i_{Lk1} , and $i_{Do3} = i_{Lm}-i_{Lk2}$. As a result, the commutation between $Do1$ and $Do3$ begins since i_{Do1} progressively grows and i_{Do3} gradually drops in accordance with (27), (29), and (30). Furthermore, since i_{Lk1} was zero in the previous mode and i_{ds2} equals i_{Lk1} in this mode. As a result, as illustrated in (28), i_{ds2} progressively rises from zero as a result of L_{k1} and L_{k2} . As a result, $M2$ can operate through gentle switching, which significantly lowers the turn-on loss. Similar to how $M2$ functions, $M1$ can be turned on in mode 8 by using the gentle switching technique. As a result, $M1$'s turn-on loss can be significantly decreased. Additionally, because this mode terminates when i_{Do3} drops to zero, there $Do3$ does not have a reverse recovery issue.

A thorough operation analysis is not included here because the operations of modes 5 through 8 are comparable to those of modes 1 through 4. The suggested converter repeats one switching cycle, going from mode 1 to mode 8.

3. ANALYSIS OF THE PROPOSED CONVERTER:

A. VOLTAGE CONVERSION RATIO:

By applying KVL to the outermost loop in Fig. 7, one can determine the voltage conversion ratio of the proposed converter: $v_{Do3} = v_{Lo}+V_o-V_{in}+v_{L2}$. The average voltage $\langle v_{Do3} \rangle$ of $Do3$ is as follows since, at

steady-state, the average voltage across the resistor is zero

$$\langle V_{Do3} \rangle = V_o - V_{in} \quad (31)$$

Do3 conducts for (1-2D) Ts+2TCM(on) during a single switching cycle, as seen in Fig. 6. Consequently, $\langle v_{Do3} \rangle$ is ascertained as follows from (5):

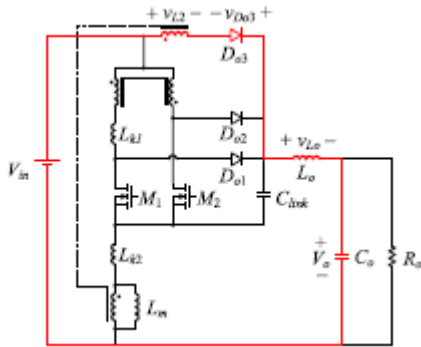


FIGURE 7. The KVL loop of the outermost path in the proposed converter.

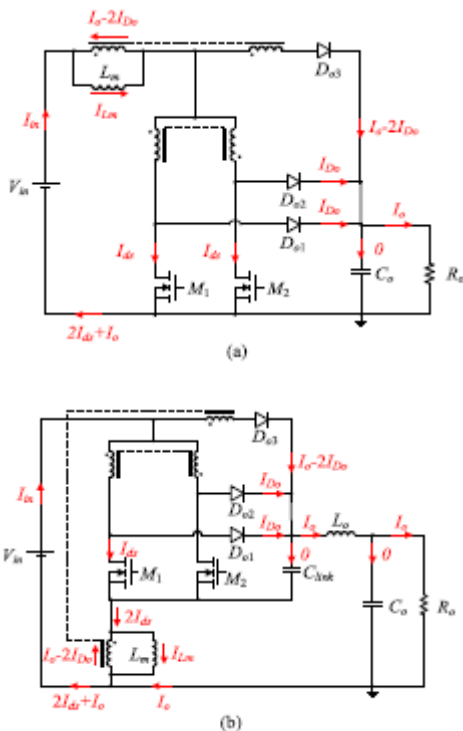


FIGURE 8. The average currents through the circuit components

- (a) Conventional converter, (b) Proposed converter.

$$\langle V_{Do3} \rangle = D_{eff} \left\{ \frac{2L_m V_{in} + L_{k2} V_o}{L_m + L_{k2}} \right\} \quad (32)$$

The voltage conversion ratio and the effective duty ratio, D_{eff} , can be calculated as follows from equations (31) and (32):

$$D_{eff} = \frac{(L_m + L_{k2})(V_o - V_{in})}{2L_m V_{in} + L_{k2} V_o} \quad (33)$$

$$\frac{V_o}{V_{in}} = \frac{L_m + L_{k2}}{L_m + (1 - D_{eff})L_{k2}} \left(1 + \frac{2L_m D_{eff}}{L_m + L_{k2}} \right) \quad (34)$$

For comparison, the voltage conversion ratio and effective duty cycle of the conventional converter are the same as those of the proposed converter because they both function in the same way.

B. COMMUTATION TIME:

As Fig. 6 illustrates, during TCM(off), the currents via Do1 and Do2 gradually drop while the current through Do3 steadily increases. Furthermore, during TCM(on), the current passing through Do1 steadily increases while the current passing through Do3 gradually drops.

$$T_{CM(off)} = \frac{i_{Lk1}(t_2)L_{k1}}{V_{Lk1}(t_2 - t_3)} \quad (35)$$

where the voltage delivered to Lk1 during mode 2 is denoted by $v_{Lk1}(t_2 - t_3)$. For the time interval $t_1 - t_2$, i_{Lk1} equals i_{ds1} , as Fig. 4(a) illustrates. The average current i_{ds1} passing through M1, assuming an ideal circuit, is $0.5I_o(V_o/V_{in} - 1)$ by KCL.

Furthermore, as illustrated in Fig. 6, $i_{ds1}(t_2)$ can be obtained as follows, presuming that the average current component of i_{ds1} during TCM(on) is insignificant because TCM(on) is significantly smaller than $D_{eff} T_s$.

$$i_{ds1}(t_2) = \frac{1}{2D_{eff}} \left(\frac{V_o}{V_{in}} - 1 \right) I_o + \frac{v_{Lk1}(t_1 - t_2)}{2L_{k1}} D_{eff} T_s \quad (36)$$

where the voltage delivered to Lk1 during mode 1 is denoted by $v_{Lk1}(t_1 - t_2)$. TCM(off) can be ascertained from (35) and (36) since $i_{Lk1}(t_2) = i_{ds1}(t_2)$.

$$T_{CM(off)} = \frac{L_{k1}+L_{k2}}{(V_o-V_{in})} \times \left[\frac{1}{2D_{eff}} \left(\frac{V_o}{V_{in}} - 1 \right) I_o + \frac{(2V_{in}-V_o)D_{eff}T_s}{8L_m+8L_{k2}+2L_{k1}} \right] \quad (37)$$

Furthermore, TCM(on) can be calculated as follows using the iLk1 waveform displayed in Fig. 6.

$$T_{CM(on)} = \frac{-vLK1(t2-t3)T_{CM(off)}-vLK1(t1-t2)D_{eff}T_s}{vLK1(t4-t5)} \quad (38)$$

where the voltage delivered to Lk1 during mode 4 is denoted by vLk1(t4-t5). The following expression for TCM(on) can be derived from (2), (10), and (38):

$$T_{CM(ON)} = \left(\frac{V_o}{V_{in}} - 1 \right) T_{CM(off)} - \frac{(L_{k1}+L_{k2})(2V_{in}-V_o)}{(4L_m+4L_{k1}+L_{k2})V_{in}} D_{eff}T_s. \quad (39)$$

For comparison, the TCM(off) and TCM(on) of the two converters are the same when the leakage and magnetizing inductances are the same, as the proposed converter and the conventional converter operate similarly.

T1 (= NT2).

C. PROPOSED CONTROL TECHNIQUES FUZZY LOGIC:

Things that are unclear or vague are referred to as fuzzy. Because we frequently find ourselves in situations in the actual world where we are unable to decide whether a condition is true or false, fuzzy logic offers incredibly useful thinking flexibility. We can then take into account the uncertainties and inaccuracies of any given situation.

Fuzzy Logic is a type of many-valued logic wherein, as opposed to merely the conventional values of true or false, the truth values of variables can be any real integer between 0 and 1. It is a mathematical technique for modeling vagueness and uncertainty in decision-making and is used to deal with imprecise or uncertain information.

Fuzzy Logic is based on the idea that in many cases, the concept of true or false is too restrictive, and that there are many shades of gray in between. It allows for partial truths, where a statement can be partially true or false, rather than fully true or false.

Fuzzy Logic is used in a wide range of applications, such as control systems, image processing, natural

language processing, medical diagnosis, and artificial intelligence.

The membership function, which indicates the extent to which an input value belongs to a certain set or category, is the core idea of fuzzy logic. A mapping from an input value to a membership degree between 0 and 1, where 0 denotes non-membership and 1 denotes full membership, is known as the membership function.

Fuzzy Rules, or if-then statements that represent the relationship between input and output variables in a fuzzy manner, are used to create fuzzy logic. A fuzzy set, or a collection of membership degrees for every potential output value, is the result of a fuzzy logic system.

4. SIMULATION RESULTS:

This part presents the experimental findings of the conventional and suggested converters based on the specification stated in Table 1, in order to verify the viability of the proposed converter. The experimental key waveforms of the two converters are presented in Figs. 9 and 2. In particular, Figs. 9(a) and (b) show the maximum output current ripple within the input voltage range for the two converters' output capacitor current ripple based on the load current at an input voltage of 36 V.

Specifically, as Fig. 9(a) illustrates, the output current ripple of the suggested converter is 4.2 A under the same load. Furthermore, Fig. 9(b) demonstrates that, at a 15 A load, the output current ripple of the proposed converter is 4.21 A, compared to 9.2 A for the conventional converter.

Additionally, as the load current rises from 10 A to 15 A, the typical converter's output current ripple rises by 4.8 A. In the meantime, regardless of the load current, that of the suggested converter stays nearly constant. Consequently, when compared to the conventional converter, the output current ripple of the suggested converter is greatly decreased.

In the meanwhile, as seen in Fig. 9(b), the typical converter's RMS current passing through the output capacitor is calculated with a 4.65 Arms load at 15 A. Meanwhile, the result RMS current of the suggested converter's capacitor is as low as 1.05 Arms, or about 4.4 times smaller than the traditional converter's. Consequently, if the same bus PCU has a capacitor, hence the lower RMS current can lessen the strain on the bus capacitor to prevent an extension of life. Furthermore, it can be argued that the suggested

converter is better suited for high-power applications since it maintains an almost constant RMS current through the output capacitor independent of the load current.

The magnetizing current waveforms of the linked inductor of the two converters, which were measured using the oscilloscope's Math function, are displayed in Fig. 9(c). With a peak magnetizing current of 18.5 A, the proposed converter is precisely 13.5 A greater than the traditional converter, which has a peak magnetizing current of 32 A. Consequently, a smaller OD234 core can be employed in the proposed converter, whereas the conventional converter requires a larger OD270 core, because the proposed converter has a lower peak magnetizing current of the linked inductor than the conventional converter. Furthermore, as illustrated in Fig. 9(d), the output inductor employed in the suggested converter has a peak current of 17.11 A, which is comparable to the 18.5 A of the proposed converter's linked inductor. Consequently, The same size OD234 magnetic inductor can be used for the proposed converter's coupling and output inductors.

coupled inductor in the proposed converter, and 0.32 T for the output inductor in the proposed converter. These values represent the maximum magnetic flux density B_{max} of the magnetic cores utilized in the two converters. Consequently, the typical converter only needs one large magnetic core, calls for two tiny magnetic cores for the connected and output inductors. Additionally, the output voltage ripple of the two converters at 36 V input voltage and 15 A full load is displayed in Fig. 9(e). As can be shown in Fig. 9(e), the suggested converter only needs two link capacitors ($C_{link} = 8 \mu F$) and three output capacitors ($C_o = 6.6 \mu F$) to maintain the output voltage ripple of both converters at about 0.45 V. In contrast, the conventional converter needs eleven output capacitors ($C_o = 24.2 \mu F$).

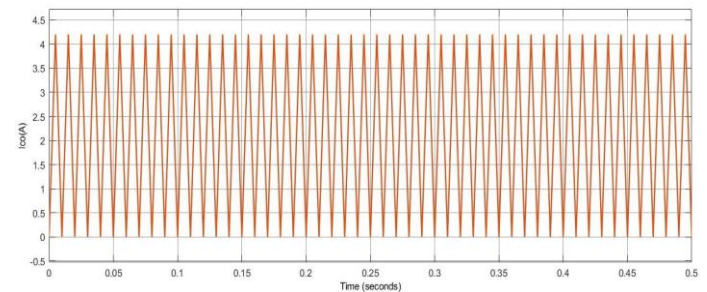
The suggested converter employs one small-coupled inductor core, one small-output inductor core, and two link capacitors, whereas the conventional converter uses one large-coupled inductor core and eleven output capacitors, capacitors, and three output capacitors.

Despite the fact that the suggested converter requires an extra magnetic while utilizing an output inductor as opposed to a traditional converter, the total quantity of capacitors needed to meet When comparing the same output voltage ripple to the typical converter, it is substantially less. Furthermore, the smaller size magnetic core can be utilized in the proposed converter since all of the inductors employed in it have peak magnetizing currents that are lower than those used in the conventional converter. As a result, the overall volume and weight of the suggested converter can be decreased. Moreover, the electrical power system of geostationary satellites often uses a number of BDRs in a parallel combination to assure dependable and powerful [28]. Thus, the suggested converter can help the electrical power system's volume and weight to be further reduced.

Parameter	Conventional converter	Proposed converter	Unit
Input voltage V_{in}	30-42		V
Output voltage V_o	50		V
Rated power P_o	750		W
Switching frequency f_{sw}	100		kHz
Transformer core	PQ2625		
Number of turns	$N_{T1} = 5$ $N_{T2} = 5$		
Leakage inductance L_{L1}	0.3		μH
Coupled inductor core	CH270125	CH234125	
Number of turns	$N_{L1} = 4$ $N_{L2} = 4$	$N_{L1} = 5$ $N_{L2} = 5$	
Magnetizing inductance L_{m1}	2.7	2.73	μH
Leakage inductance L_{L2}	0.24	0.29	μH
Output inductor core	-	CH234125	
Output inductance L_o	-	5.36	μH
Output capacitor	MKT1820522015 (2.2 μF)		
Output capacitance C_o	24.2	6.6	μF
Link capacitor	RA4405K100-FA (4 μF)		
Link capacitance C_{link}	-	8	μF

TABLE 1. Parameters used in the experiment.

smaller core than the one found in a traditional converter. The B_{max} values of the coupled inductor in the conventional converter are 0.317 T, 0.247 T for the



(a)

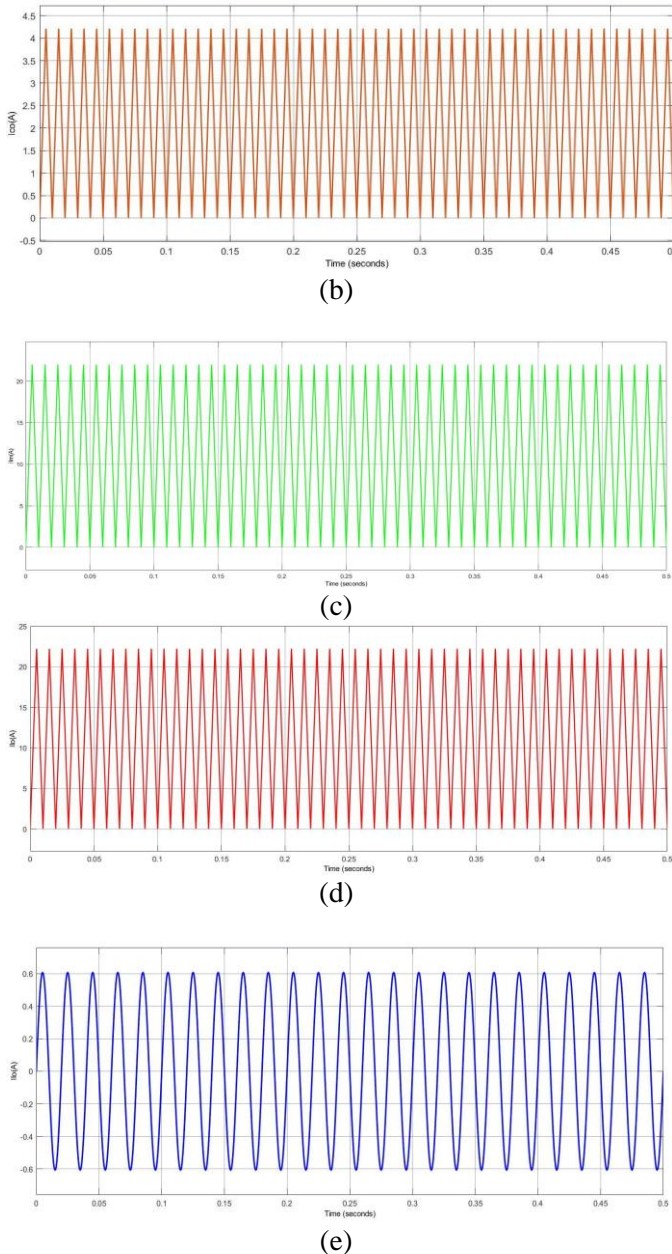


FIGURE 9. The experimental key waveforms (a) Output capacitor current ripple at 10 A load, (b) Output capacitor current ripple at 15 A load, (c) Magnetizing current of the coupled inductor

VI. CONCLUSION:

The present study proposes an enhanced Weinberg converter designed to address the shortcomings of the traditional Weinberg converter. More specifically, because of the output inductor, the suggested converter can considerably lower the output current ripple when compared to the standard converter. As a result, in comparison to a typical converter, a substantially less number of output capacitors are needed to get the same

output voltage ripple. Additionally, the suggested converter's output capacitor root mean square (RMS) current is significantly lower than the traditional converter's.

Therefore, the suggested converter can lessen the load on the output capacitor if the same output capacitance is utilized in both converters. Furthermore, the suggested converter maintains a nearly constant output current ripple even as the load current increases. In the meanwhile, the The typical converter's output current ripple rises in direct proportion to the load current rises. Consequently, it can be said that the suggested converter is more appropriate because it keeps the output current ripple nearly constant independent of the load current for applications requiring a lot of power. On the other hand, the suggested converter necessitates an extra magnetic component for the output inductor in contrast to the traditional converter. On the other hand, the linked inducer's peak magnetizing current in the suggested converter is about half that of the typical converter. As a result, in comparison to the conventional converter, the suggested converter can avoid magnetic core saturation even at greater loads and minimize the magnetic core's size.

Furthermore, a 750 W-rated prototype built using the optimally planned parameters was used to validate the suggested converter.

Three aspects in particular allow the proposed converter to achieve high efficiency: the switches' soft switching operation, the lack of the diodes' reverse recovery difficulty, and the loss analysis-based optimal design of the magnetic components. More specifically, for input voltages of 30 V, 36 V, and 42 V, the suggested converter achieves an efficiency of at least 92.9% throughout the whole load range. Also, because there are fewer output capacitors and smaller magnetic components, the suggested converter can lower the total weight of the typical converter from 404 g to 392 g.

The suggested converter will have a greater weight reduction impact because numerous BDRs are typically utilized in parallel combinations to achieve dependability, redundancy, and higher power. Based on these findings, it is projected that the suggested converter will be appropriate for high-power applications, accomplish the weight reduction and shrinking of electrical power systems for geostationary satellites, and lower the cost of satellite launch.

REFERENCES:

- [1] R. Emrick, P. Cruz, N. B. Carvalho, S. Gao, G. Quay, and P. Waltereit, "The sky's the limit: Key technology and market trends in satellite communications," *IEEE Microw. Mag.*, vol. 15, no. 2, pp. 65–78, Mar. 2014.
- [2] Satellite Industry Association. State of the Satellite Industry Report. Accessed: Jun. 2022. [Online]. Available: <http://www.sia.org>
- [3] C. Wang, D. Bian, S. Shi, J. Xu, and G. Zhang, "A novel cognitive satellite network with GEO and LEO broadband systems in the downlink case," *IEEE Access*, vol. 6, pp. 25987–26000, 2018.
- [4] M. Nitti, M. Murrioni, M. Fadda, and L. Atzori, "Exploiting social Internet of Things features in cognitive radio," *IEEE Access*, vol. 4, pp. 9204–9212, 2016.
- [5] A. Gupta and R. K. Jha, "A survey of 5G network: Architecture and emerging technologies," *IEEE Access*, vol. 3, pp. 1206–1232, 2015.
- [6] J. Foust, "SpaceX's space-Internet woes: Despite technical glitches, the company plans to launch the first of nearly 12,000 satellites in 2019," *IEEE Spectr.*, vol. 56, no. 1, pp. 50–51, Jan. 2019.
- [7] M. Harris, "Tech giants race to build orbital Internet [news]," *IEEE Spectr.*, vol. 55, no. 6, pp. 10–11, Jun. 2018.
- [8] P. Bizony, "Hollydays in space/space tourism," *Eng. Technol.*, vol. 3, no. 13, pp. 22–25, Aug. 2008.
- [9] M. R. Patel, *Spacecraft Power Systems*. Boca Raton, FL, USA: CRC Press, 2005.
- [10] D. Pidgeon, K. M. Price, and A. Tsao, "Mass and power modeling of communication satellites," Lewis Res. Center, Cleveland, OH, USA, Tech. Rep. NASA CR-189186, 1991.
- [11] H. W. Jones, "The recent large reduction in space launch cost," in *Proc. 48th Int. Conf. Environ. Syst.*, Jul. 2018, pp. 8–12.
- [12] J. Park, J. Han, S. Choi, and G. Moon, "Two-switch forward converter with an integrated buck converter for high bus voltage in satellites," *IEEE Trans. Power Electron.*, vol. 38, no. 2, pp. 2041–2051, Feb. 2023.
- [13] H. Nagata and M. Uno, "Nonisolated PWM three-port converter realizing reduced circuit volume for satellite electrical power systems," *IEEE Trans. Aerosp. Electron. Syst.*, vol. 56, no. 5, pp. 3394–3408, Oct. 2020.
- [14] H. Zhu and D. Zhang, "Design considerations of sequential switching shunt regulator for high-power applications," *IEEE Trans. Ind. Electron.*, vol. 67, no. 11, pp. 9358–9369, Nov. 2020.
- [15] H. A. Weinberg and J. Schreuders, "A high-power high-voltage DC–DC converter for space application," *IEEE Trans. Power Electron.*, vol. PE-1, no. 3, pp. 148–160, Jul. 1986.
- [16] M. Koziol, "Geostationary satellites for small jobs," *IEEE Spectr.*, vol. 57, no. 1, pp. 48–58, Jan. 2020.
- [17] D. W. Sun, F. Ellmers, A. Winkler, H. Schuff, and M. J. S. Chamarro, "European small geostationary communications satellites," *Acta Astronautica*, vol. 68, nos. 7–8, pp. 802–810, Apr. 2011.
- [18] M. Iwasa, H. Kusawake, S. Shimada, A. Ishii, Y. Kikuchi, K. Aoki, J. Shimizu, and T. Ito, "Lightweight power control units and power distribution control unit for satellites," *J. Space Technol. Sci.*, vol. 28, no. 1, pp. 30–36, 2013.
- [19] J. Lee, E. Kim, and K. G. Shin, "Design and management of satellite power systems," in *Proc. IEEE 34th Real-Time Syst. Symp.*, Vancouver, BC, Canada, Dec. 2013, pp. 97–106.
- [20] O. Shekoofa and E. Kosari, "Comparing the topologies of satellite electrical power subsystem based on system level specifications," in *Proc. 6th Int. Conf. Recent Adv. Space Technol. (RAST)*, Istanbul, Turkey, Jun. 2013, pp. 671–675.
- [21] J. Park, J. Han, K. Park, B. Lee, and G. Moon, "A new direct charging control for electrical power systems in low earth orbit satellites," *IEEE Trans. Aerosp. Electron. Syst.*, early access, Oct. 31, 2022, doi:10.1109/TAES.2022.3218495.
- [22] Z. Hong-Yu, Z. Bo-Wen, and Z. Dong-Lai, "Overview of architectures for satellite's regulated bus power system," in *Proc. IEEE 1st China Int. Youth Conf. Electr. Eng. (CIYCEE)*, Wuhan, China, Nov. 2020, pp. 1–8.
- [23] A. Garrigos, J. A. Carrasco, J. M. Blanes, and E. Sanchis-Kilders, "A power conditioning unit for high power GEO satellites based on the sequential switching shunt series regulator," in *Proc. IEEE Medit.*

Electrotech. Conf. (MELECON), Malaga, Spain, 2006, pp. 1186–1189.

[24] E. Maset, J. B. Ejea, A. Ferreres, E. Sanchis-Kilders, J. Jordan, and V. Esteve, “High-efficiency Weinberg converter for battery discharging in aerospace applications,” in Proc. 21st Annu. IEEE Appl. Power Electron. Conf. Expo. (APEC), Dallas, TX, USA, 2006, p. 7.

[25] A. H. Weinberg, “The battery discharge regulator of the Galileo satellite test bed-v2/a power system using the Weinberg topology,” presented at the 7th Eur. Space Power Conf., Stresa, Italy, May 2005.

[26] E. Maset, A. Ferreres, J. B. Ejea, E. Sanchis-Kilders, J. Jordan, and V. Esteve, “5 kw Weinberg converter for

battery discharging in highpower communication satellites,” in Proc. IEEE 36th Power Electron.Spec. Conf., Dresden, Germany, Jun. 2005, pp. 69–75.

[27] A. K. Weinberg and P. R. Boldo, “A high power, high frequency, DC to DC converter for space applications,” in Proc. 23rd Annu. IEEE Power Electron. Spec. Conf. (PESC), Toledo, Spain, vol. 2, Jun. 1992, pp. 1140–1147.

[28] J. B. Ejea, A. Ferreres, E. Sanchis-Kilders, E. Maset, V. Esteve, J. Jordán, and A. Garrigos, “Optimized topology for high efficiency battery discharge regulator,” IEEE Trans. Aerosp. Electron. Syst., vol. 44, no. 4, pp. 1511–1521, Oct. 2008.